REPORT OF INVESTIGATIONS/1994

Effect of Dead-End Crosscuts on Contaminant Travel Times in Mine Entries

By G. F. Friel, J. C. Edwards, and G. S. Morrow

UNITED STATES DEPARTMENT OF THE INTERIOR

BUREAU OF MINES

U.S. Department of the Interior
Mission Statement

As the Nation's principal conservation agency, the Department of the Interior has responsibility for most of our nationally-owned public lands and natural resources. This includes fostering sound use of our land and water resources; protecting our fish, wildlife, and biological diversity; preserving the environmental and cultural values of our national parks and historical places; and providing for the enjoyment of life through outdoor recreation. The Department assesses our energy and mineral resources and works to ensure that their development is in the best interests of all our people by encouraging stewardship and citizen participation in their care. The Department also has a major responsibility for American Indian reservation communities and for people who live in island territories under U.S. administration.

Cover: CO sensor in entry near location of CO injector.

Report of Investigations 9517

Effect on Dead-End Crosscuts on Contaminant Travel Times in Mine Entries

By G. F. Friel, J. C. Edwards, and G. S. Morrow

UNITED STATES DEPARTMENT OF THE INTERIOR
Bruce Babbitt, Secretary

BUREAU OF MINES
Rhea L. Graham, Director

International Standard Serial Number
ISSN 1066-5552

CONTENTS

ILLUSTRATIONS

TABLES

UNIT OF MEASURE ABBREVIATIONS USED IN THIS REPORT

cm	centimeter	m^3/min	cubic meter per minute
g	gram	m^3/s	cubic meter per second
kPa	kilopascal	min	minute
m	meter	ppm	part per million
m/s	meter per second	ppm/s	part per million per second
m^2/s	square meter per second	s	second

Reference to specific products does not imply endorsement by the U.S. Bureau of Mines.

EFFECT OF DEAD-END CROSSCUTS ON CONTAMINANT TRAVEL TIMES IN MINE ENTRIES

By G. F. Friel,[1] J. C. Edwards,[2] and G. S. Morrow[3]

ABSTRACT

A series of experiments in the U.S. Bureau of Mines Safety Research Coal Mine at the Pittsburgh Research Center evaluated the effects of crosscuts on the travel time of carbon monoxide (CO) along an entry to improve the accuracy of a mine-fire locator program. Three entries, ten single crosscuts, and three double crosscuts were instrumented with CO sensors. One-percent CO in nitrogen was released and monitored as it traveled the entries. In addition to dispersion of CO at the front of the CO wave, CO was entrained from the entry into the crosscuts. It was determined for an entry and single-crosscut configuration that the measured travel time for a concentration change of 5 ppm was 27% greater than the predicted time based upon entry volume only, but 13% less than the predicted time based upon entry and crosscut volumes. For an entry and double-crosscut configuration, the measured travel time for the same concentration change was 25% greater than the predicted time based upon entry volume only, but 10% less than the predicted time based upon entry and crosscut volumes. An effective dispersion coefficient for CO dispersion along one of the entries was estimated to be 1.5 m^2/s.

[1]Chemical engineer.
[2]Research physicist.
[3]Electronics technician.
Pittsburgh Research Center, U.S. Bureau of Mines, Pittsburgh, PA.

INTRODUCTION

The strategy adopted for mine-fire detection and early warning depends, in large measure, upon the ability to interpret fire signatures. Early detection of a fire is primarily accomplished with smoke detectors (ionization or optical types) and carbon monoxide (CO) detectors. Appropriate alarm levels are set for either type of detector to discriminate against false alarms commonly induced in smoke detectors by airborne dust and in CO detectors by diesel exhaust or desorption from gob areas. Once reliable detectors and alarm threshold levels have been selected, the rapid determination of the location of a fire in a mine from detector alarms can be critical for the safe evacuation of miners and the successful extinguishment of the fire.

Travel times of contaminants (CO, smoke, etc.) at sensors in a mine-monitoring network can be used to estimate the location of a fire in a mine (*1-2*).[4] Previous analysis (*2*) tacitly assumed a lack of contaminant dispersion due to turbulent flow and dilution by the dead-end crosscuts. A comparison was made by Cohen (*3*) of measured CO concentration from experimental CO releases in a working mine with the results of computations from the ventilation program of Edwards and other (*4*). Cohen adjusted the definition of entry cross-sectional area and perimeter to produce a contaminant velocity that mainly accounted for contaminant dispersion and air dilution of contaminants by dead-end crosscuts. Utilization of a U.S. Bureau of Mines (USBM) ventilation computer program for underground mines (*4-6*) determined airflows in the network from natural ventilation, fan characteristic curves, and airway resistance. However, computer-program changes in the entry cross-sectional area and perimeter to adjust the air travel time to fit the contaminant travel time require that the friction factor also be adjusted to maintain the calculated resistance and mass flow rate. An alternative method is to develop contaminant travel times as a subsidiary calculation that automatically adjusts the cross-sectional area, perimeter, and friction factor based on mine geometric data for accurate travel-time and heat-transfer calculations. Litton and others (*7*) suggested a correlation to predict contaminant travel times given geometric variables of an entry and its crosscuts, but little experimental data existed to support this correlation. The goal of this study by the USBM was to supply data to either support the conjecture by Litton and others (*7*) or to formulate a different correlation, possibly with more significant variables, that could be used in a mine-fire-locator computer program that would improve mining safety.

EXPERIMENTAL CONFIGURATIONS

A series of experiments was conducted in the Safety Research Coal Mine (SRCM) to investigate the response of a network of CO sensors to a controlled release of CO. Three entries (B Butt, C Butt, and F Butt) shown in figures 1 and 2, were intersected by dead-end crosscuts formed by positioning brattices across rooms on one or both sides of the entry. The ventilation was controlled by a Joy axivane exhaust fan at the top of a 6-m vertical shaft. The flow quantity within the entries for all the experiments ranged from 5.7 to 10.4 m^3/s. Six different experimental configurations were investigated.

In the first configuration, four experiments (A through D) were conducted with CO sensors distributed along B Butt, C Butt, and in several single crosscuts. Carbon monoxide was released at the beginning of B Butt. Rooms 6 through 12 and 15 were accessible. Rooms 14 and 16 were isolated with brattices.

In the second configuration a single experiment, experiment E, was conducted with sensors positioned in B and C Butts and with all crosscuts blocked. This provided a comparison experiment for CO dispersion without entrainment into crosscuts. The CO also was released at the beginning of B Butt.

In the third (experiment F) and fourth configurations (experiments G through I), the CO was released at the beginning of C Butt. Rooms 15 and 16 were accessible in experiment F. Rooms 14 to 16 were accessible in experiments G through I.

For the fifth configuration (experiments J through L), sensors were positioned along F Butt and within the crosscuts. The CO was released about 3 m from the beginning of F Butt. Both sides of the double crosscuts were bratticed to the same depths on the left as on the right of the entry. In the downwind direction these depths were 15.7 m, 8.5 m, and 4.4 m, respectively. For the sixth configuration (experiment M), all crosscuts along F Butt were bratticed off in a manner similar to experiment E.

[4]Italic numbers in parentheses refer to items in the list of references preceding the appendixes.

Figure 1

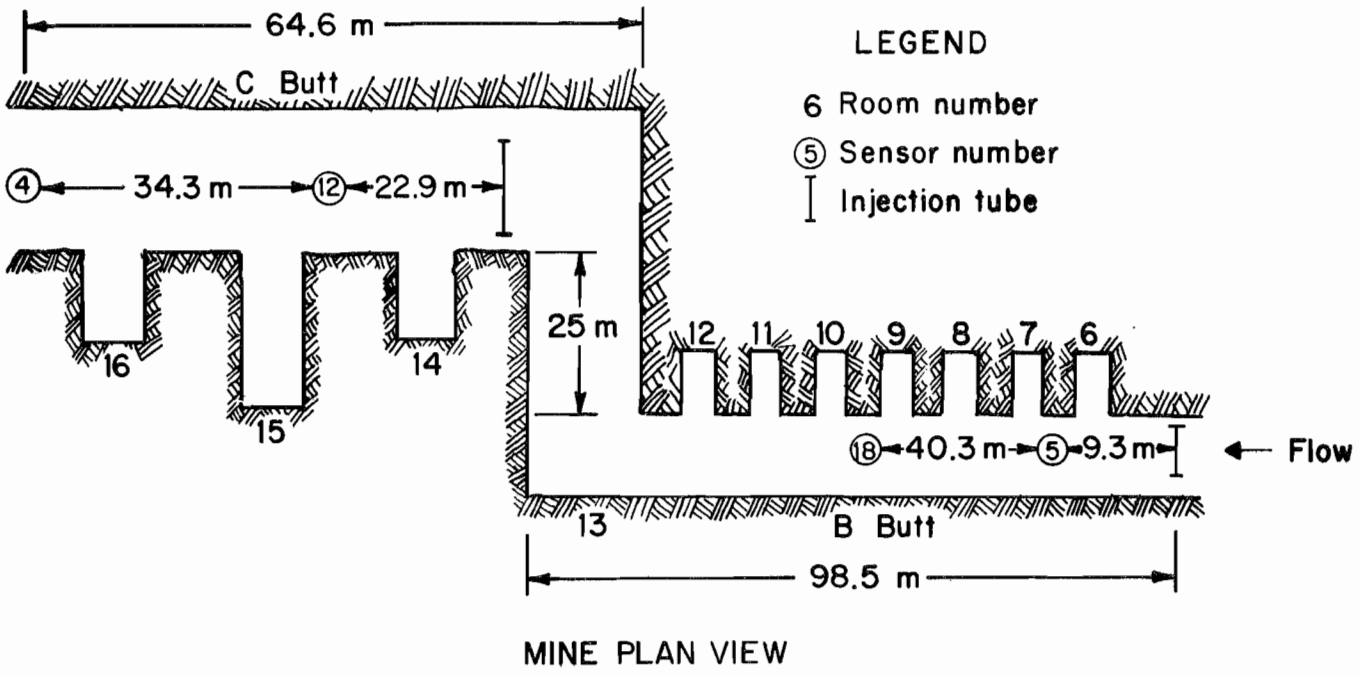

Diagram of mine entries and single dead-end crosscuts.

Figure 2

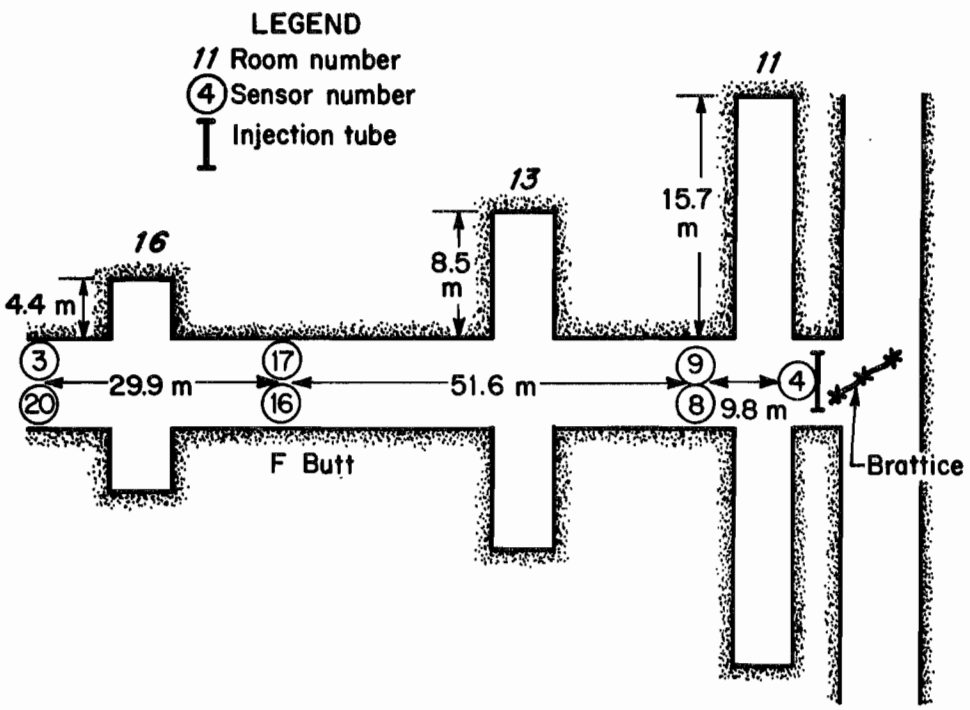

Diagram of mine entry and double dead-end crosscuts.

Entry sensors common to experiments A through E, which utilized both B Butt and C Butt, as well as experiments F through I, which utilized only C Butt, are shown in figure 1. Sensors common to experiments J through M in F Butt are shown in figure 2. Sensor 4, shown in both figures 1 and 2, was moved from C Butt to F Butt for the latter experiments.

The average width and height of B Butt were 3 m and 2.1 m, of C Butt were 4.3 m and 2 m, and of F Butt were 4.7 m and 2 m, respectively. The part of B Butt used, from the CO injector to room 13, was 98.5 m long. The length of C Butt was 64.6 m from room 13 to the last sensor in C Butt. The length of F Butt was 94.3 m from the CO injector to the last downwind sensor. The injector was 3 m from the first downwind sensor in F Butt. Rooms 6 through 12 along B Butt had an average height, width, and depth of 2.1 m, 2.8 m, and 5.2 m, respectively. Rooms 14 through 16 along C Butt had an average height and width of 1.9 m and 4.3 m. Rooms 11, 13, and 16 along F Butt had an average height and width of 2.0 m and 4.4 m. For the first configuration, room 15 was 22.2 m deep, as shown in figure 3. For the third configuration, a brattice was removed from room 16 exposing a depth of 9.4 m, as shown in figure 4. For the fourth configuration, brattices were removed from rooms 14 and 16, and all the room depths in C Butt were set to 9.4 m. Room 13 had an average height, width, and length of 1.8 m, 4.0 m, and 25 m, respectively. Dimensions, area ratios, and volume ratios are summarized in table 1 for four sensor paths. The effect of crosscuts on contaminant travel times will be described later for these selected paths. The average crosscut cross-sectional area is A_c, and the average entry cross-sectional area is A_e for each path specified. The sum of the crosscut volumes is V_c, and the entry volume is V_e between the sensors specified.

For each experiment with crosscuts open to the entry, sensors were located in selected dead-end crosscuts along B, C, and F Butts. In experiments A through D, two sensors each were located in rooms 9 and 12, and three sensors were located in room 15 for all experiments conducted within both B and C Butts. The sensor configuration in room 15 for this series of experiments is shown in figure 3. In experiment D, sensors also were located in rooms 10 and 13. In experiments F through I, conducted in C Butt, room 16 was open and had two sensors as shown in figure 4. In experiments E through I, sensors were distributed over the cross section of the entries at selected locations to ascertain the uniformity of the CO concentration over the airway cross section. In experiments J through M, conducted in F Butt, sensors were located in rooms 11, 13, and 16. For each experiment a sensor was maintained upwind of the injector to monitor ambient CO concentration during the experiment.

Table 1.—Dimensions, area ratios, and volume ratios

Entries	Path	Width, m	Height, m
B Butt	5 → 18	2.81	1.93
C Butt	12 → 4	4.42	1.97
F Butt	8 → 16	4.88	1.98
	16 → 20	4.57	1.98
Experiments	**Path**	**V_c/V_e**	**A_c/A_e**
A through D	5 → 18	0.42	1.08
	12 → 4	0.61	0.94
F through I	12 → 4	0.51	0.94
J through L	8 → 16	0.30	0.91
	16 → 20	0.29	0.97

Notes: Numbers under Path refer to sensors.
V_c is volume of crosscuts between sensors.
V_e is volume of entry between sensors.
A_c is cross-sectional area of crosscuts.
A_e is cross-sectional area of entry.

Figure 3

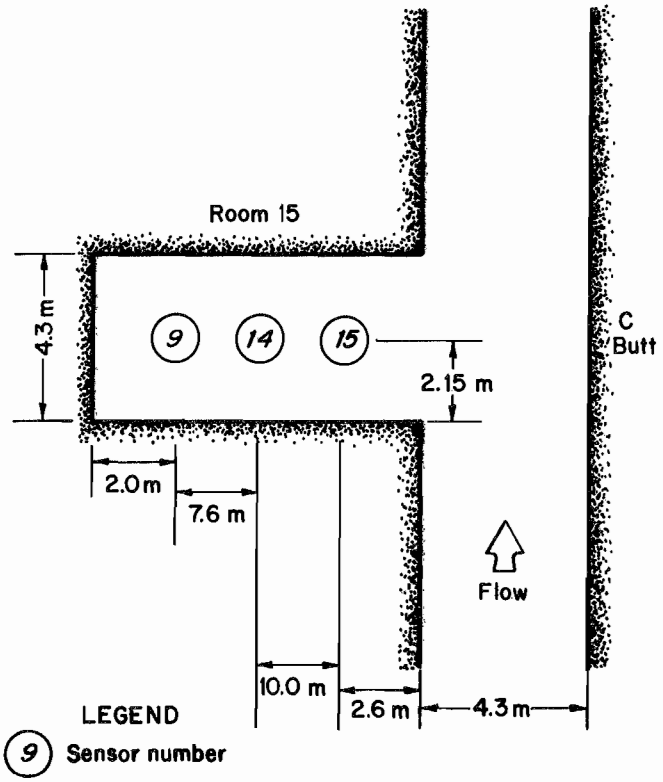

Diagram of room 15 in C Butt.

Figure 4

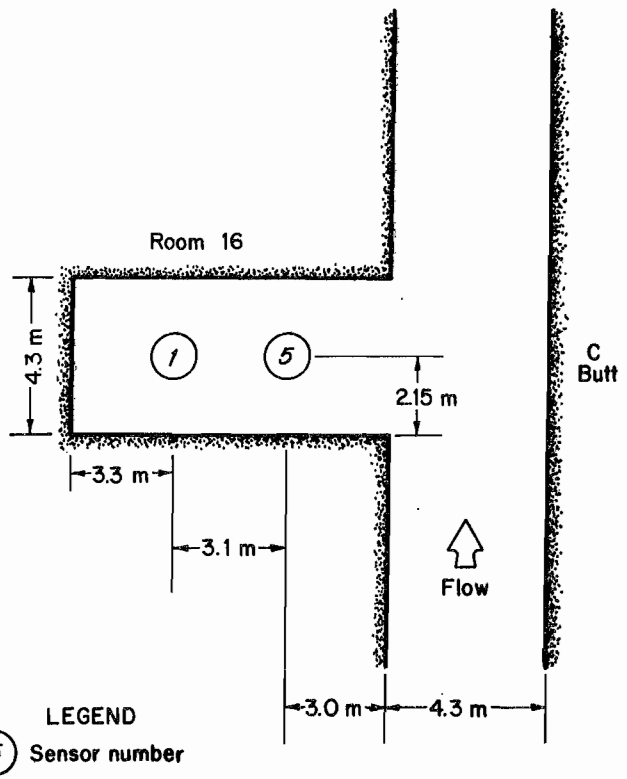

Diagram of room 16 in C Butt.

EXPERIMENTAL PROCEDURE

Prior to the release of the CO for each experiment, a ventilation survey was made of the entries. Smoke-tube measurements were made within selected crosscuts. In particular, the ventilation was measured at several locations where the entry narrowed, as well as 1.8 m upstream of the sensors, and at the CO injection location. Since most velocity measurements contained wind and fan fluctuations, 5- and 9-point, time-averaged flow measurements were made during the ventilation survey. Temperature, pressure, and humidity data also were recorded.

One-percent CO in nitrogen was injected into the entries from a cylinder containing 0.045 m^3 of the gas mixture pressurized to about 10,000 kPa. The gas was distributed across the entry during experiments in B and C Butts through a 10-cm-diam, perforated plastic tube 2.5 m long that was oriented perpendicular to the airflow direction. The tube was suspended in a horizontal position at midheight and in the middle of the entry. The gas pressure from the cylinder was reduced through a regulator to a safe level of about 700-kPa gauge pressure before flowing through a 2-m aluminum tube, with an inside diameter of about 1 cm, to the distribution tube. Except for brief periods at the start and end of injection, the flow rate of CO into the entry was constant. These conditions resulted in an injection period of about 5 min when about 50 g of CO was injected before the cylinder was nearly empty. Since the flow rate of the cylinder gas was less than 0.2% of the entry air flow rate, the cylinder-gas flow rate was nearly two orders of magnitude less than the flow-rate variations created by wind and fan fluctuations and was not added to the measured values of the entry air flow rate. When the experiments were shifted into F Butt, it was found by feeling the pressure of injection along the distribution tube that the tube was inadequate to distribute gas evenly in this section of the mine. This nonuniformity of injection in F Butt was caused by nonuniform pressure

changes along the distribution tube produced by entry air flowing around a nearby right-angle turn. A new 5-cm-diam steel tube to inject the gas was made 3 m long and with smaller distribution holes. This tube was subjected to a higher pressure during injection that produced a calculated gauge pressure of more than 100 kPa at the distribution holes. As a result of these modifications, and assuming nearly adiabatic conditions during the short time the gas flowed through the distribution holes, the gas exited the distribution tube at a steady sonic velocity of about 340 m/s and produced a measured injection period of about half of the previous periods, or 2.5 min. Since the entry air-pressure changes along the distribution tube were a small fraction of the pressure drop from the distribution holes, the flow rates of CO from the distribution holes were essentially independent of the local air-pressure changes in F Butt yielding a more even CO distribution across the entry. This tube was then used for experiments I through M. Also, a brattice was positioned at the entrance to F Butt by trial and error so the bulk air-velocity distribution at the injector was nearly uniform. Conspec model PL1400-LC CO-diffusion sensors were used for CO detection, while the concentration data were collected by a Conspec monitoring system at 2-s intervals. Calibration gas of 25-ppm CO in nitrogen was used to calibrate the Conspec sensors. The full-scale indication of the CO sensors was 50 ppm.

All of the roof sensors were suspended freely on hooks. The openings of the sensor diffusion tubes were approximately 0.4 m from the roof with a 20° tilt of the diffusion tubes from a vertical line into the upwind air and with the openings facing downward. These sensor positions were based upon previous experiments with diffusion-mode sensors that showed that the sensor response was affected by the position of the sensor with reference to the direction of the gas velocity flowing past the sensor. It was found that a sensor indicated a higher, more accurate value near the full-scale CO concentration and the response was more rapid if an upwind rather than a downwind tilt was given to the sensor. Floor sensors were also given the same upwind tilt to their diffusion tubes and positioned with the diffusion-tube openings 0.4 m from the floor. Because of these findings, the travel time between a CO source and a sensor at the level of 5-ppm CO above ambient CO concentration (Δ5 ppm) for a sensor positioned facing slightly upwind should be less than the travel time for a sensor facing downwind.

RESULTS

TRAVEL-TIME CORRELATIONS

During the injection period, the injected CO mixture was colder than the humid ventilation air and produced frost on the injection tubing. This cooling indicated that the Joule-Thomson coefficient, $(\partial T/\partial P)_E$, for the injection conditions was positive. Therefore, most of the CO mixture initially flowed toward the mine-entry floor before turbulent mixing redistributed the gas uniformly downwind.

Several overall trends emerged from an analysis of the experimental data. The CO profile in the entry was reduced in slope (time rate of change of CO concentration) by dispersion due to air turbulence as the CO traversed the entry as well as by entrainment into the crosscuts. The sensors in the dead-end crosscuts indicated CO was entrained into the crosscuts. The induced rotation of the air in the crosscuts that produced most of the entrainment was observed with smoke-tube releases.

Typical CO-concentration profiles recorded for a CO release in B Butt during experiment C by pairs of entry sensors are shown in figure 5. This figure shows the concentrations versus time for sensors 5 and 18 in B Butt and for sensors 12 and 4 in C Butt. Similar profiles occurred for CO released in C and F Butts. The time to the initial sensor response cannot be considered significant because data collection was initiated before the CO release to indicate the stability of the ambient CO concentration. By using differences between identical sensor concentrations to determine the travel times, the delays caused by the arbitrary start time together with the dynamics of the sensors and the injection distributor would cancel each other. The plateau of each concentration curve exhibited considerable raggedness. Since the magnitude and period of entry air-velocity variations appeared similar to CO-concentration variations, the most likely cause of the raggedness on the concentration curves was the effect of fan and atmospheric wind fluctuations on entry air velocity.

Although CO dispersion associated with the entry Reynolds number will gradually flatten the concentration profile with travel distance, a more immediate effect is the entrainment of CO into the crosscuts and the lowering of the overall CO-concentration profile. This lowering effect is illustrated in figure 6, which displays the results of sensors 12 and 4 in experiment H in which rooms 15 and 16 in C Butt were open. The entrainment not only lowers the concentration curve of sensor 4 with respect to the curve for sensor 12, but decreases the rate of rise of the sensor-4 concentration curve with respect to time. The

Figure 5

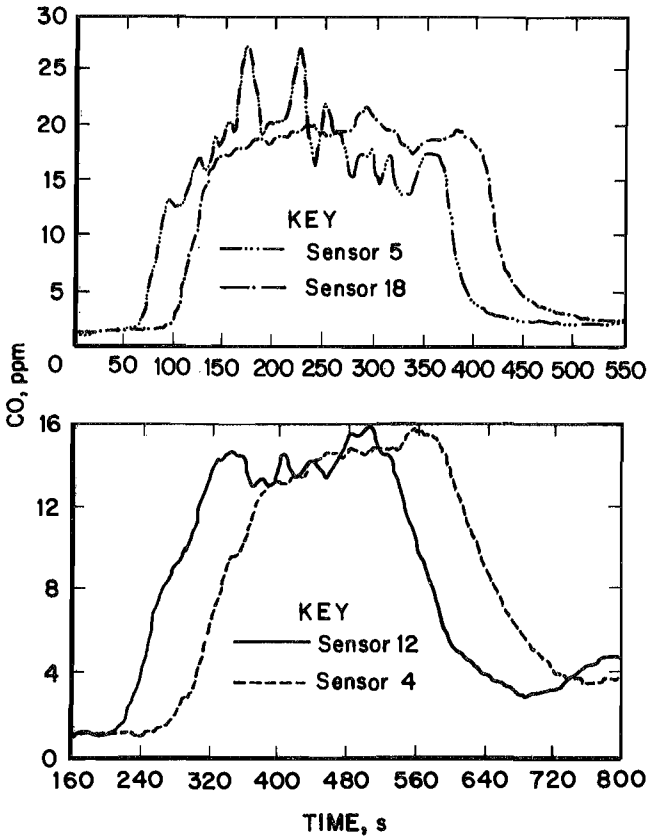

CO concentration for experiment C, top, at sensors 5 and 18 in B Butt; and bottom, at sensors 12 and 4 in C Butt.

Figure 6

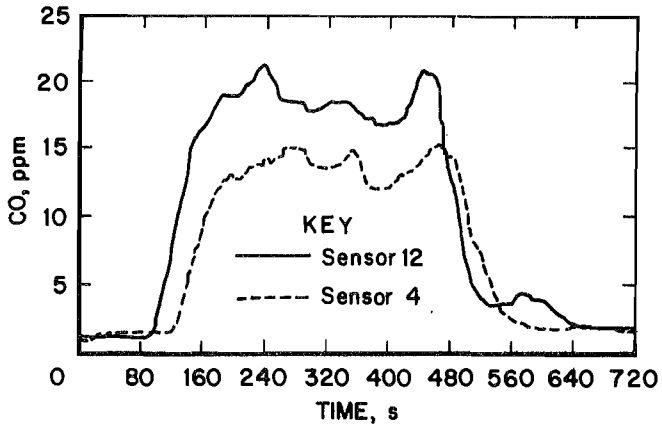

CO concentration at sensors 12 and 4 in C Butt for experiment H.

Figure 7

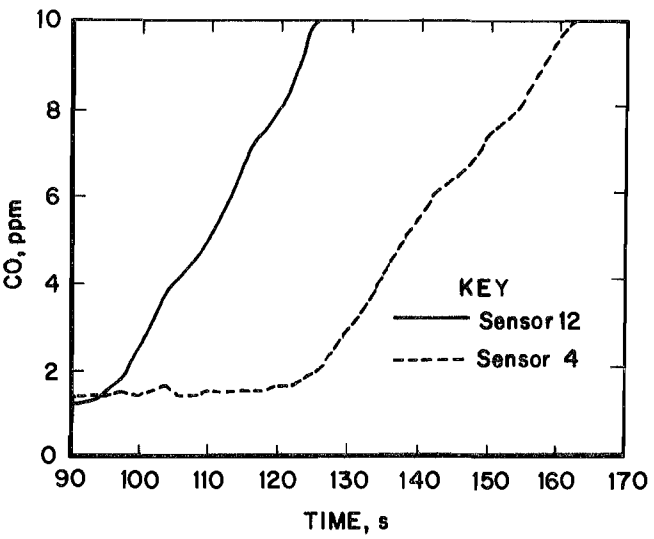

Magnified view of a portion of figure 6.

difference between the slopes of these curves during the period of increasing CO concentration is shown magnified in figure 7. The average slope of the sensor-12 curve between 100 s and 120 s is 0.30 ppm/s. The slope of the sensor-4 curve between 130 s and 160 s is 0.23 ppm/s. Although this difference in slopes is relatively small because of the relatively small experimental region of the SRCM, the difference could be substantially greater in larger underground mining regions.

The velocity of air rotating within the crosscuts was measured about 1 m from the rib of a crosscut and about half of the crosscut width inside the crosscut using the smoke-tube method. Velocity values within the crosscuts were found to range from 0.2 m/s to 0.3 m/s for average entry air velocities past the crosscuts ranging from 1.0 m/s to 1.5 m/s. Below 1.0 m/s entry air velocities, the velocities of air in the crosscuts were so small that vibrational turbulence in the crosscuts, caused by the fan vibrations and eddy oscillations, dissipated smoke relatively quickly and prevented accurate visual measurement. The deeper crosscuts, 9.4 m to 22.2 m in C butt and 8.5 m to 15.7 m in F Butt, compared with the shallower crosscuts, 5.2 m in B Butt and 4.4 m in F Butt, did not display significant rotational motion near the back of the crosscuts. Figures 8 and 9 show the measured CO concentrations in room 15 for experiment D and room 16 for experiment H, respectively. In figure 8, the velocity at which the maximum CO concentration traveled into room 15 was approximately constant at 0.1 m/s between the three sensors in room 15.

Figure 8

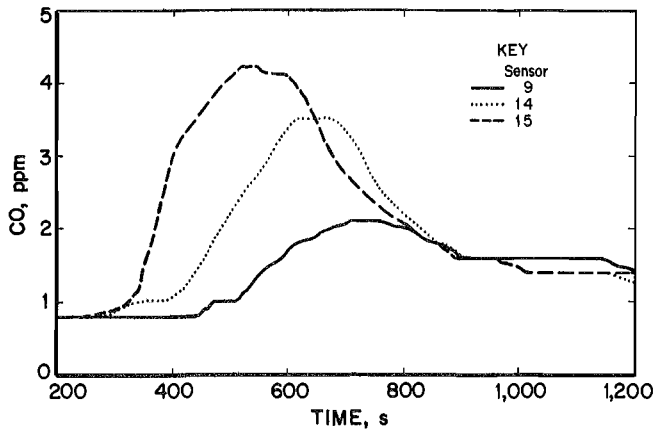

CO concentration at sensors 15, 14, and 9 in room 15 for experiment D.

Figure 9

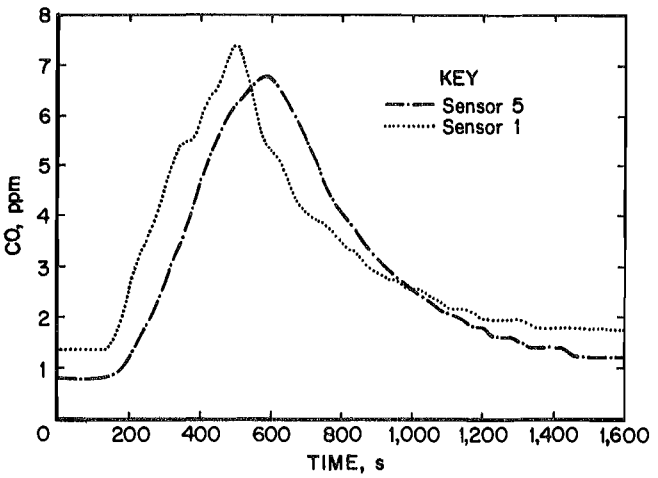

CO concentration at sensors 5 and 1 in room 16 for experiment H.

This CO velocity, however, was a complex mix of bulk rotational motion and turbulent dispersion between the three sensors. The crosscut concentration curves in figure 8 approximated an asymptotic exponential increase and decrease over the time range in the figure. By analogy, these concentration profiles are similar to the charge-versus-time profile of a charging and a discharging electrical capacitor. The return to ambient CO concentration at a rate significantly slower than the rate of rise in CO concentration in figure 8 was probably caused by the crosscuts upwind of room 15 returning CO to the entry, which in turn would impede the flow of CO from the downwind crosscuts. To a lesser extent, this phenomenon is caused by the upwind and room-15 surface areas desorbing CO that had been absorbed. The concentration of CO returned to its original ambient value of 0.8 ppm at about 2,500 s. In figure 9, the relatively constant rate of increase in CO concentration at sensors 1 and 5 occurs over nearly the same time period that the CO wave is recorded by sensors 12 and 4 in figure 6 for experiment H. This constant rate of increase in CO concentration at sensors 1 and 5 in figure 9 would be expected with the relatively flat plateaus on the curves for sensors 4 and 12 in figure 6. A constant vertical separation between the concentration curves for sensors 4 and 12 with a constant entry flow rate would mean that CO was flowing at a constant rate from C Butt into room 16. As soon as the CO wave passed the front of room 16, the concentration recorded by sensors 1 and 5 fell off asymptotically. The changes in concentration at sensor 5 lagged behind the changes in concentration at sensor 1 because the CO from C Butt reaching sensor 5 did so mainly through the slower mechanisms of diffusion and turbulent dispersion toward the center of the rotating air mass within the crosscut where sensor 5 was likely located, while the location of sensor 1 was probably in the rim of the rotating air mass.

A significant result of the entrainment of CO in the crosscuts was to increase the travel time between two mine locations for a specific CO concentration. Since the entrainment of CO into the crosscuts effectively lowers the concentration-versus-time curve, the specific concentration on the curve is shifted forward in time as the curve is lowered. For example, the decrease in the plateau CO concentration from the curve for sensor 12 to the curve for sensor 4 in figure 6 caused the time difference between the curves at a specific concentration to be increased above what the time difference would have been had the plateau concentrations of the two curves been the same.

As part of the data analysis for each experiment, the time of first arrival of CO at each sensor, and the time of arrival of a specific concentration of CO at each sensor, were recorded. The time lapse between entry-sensor records were compared with travel times predicted from ventilation measurements. For all the experiments, the measured CO travel times, τ_m, between pairs of sensors are tabulated in table 2 for the two cases of CO first arrival and $\Delta 5$ ppm. The travel times determined by first arrival of CO were greater than the travel times from $\Delta 5$-ppm data for three of the sensor pairs because air-velocity noise made the determination of the first-arrival time of CO somewhat subjective. The value of $\Delta 5$ ppm was selected because of the nearly linear rise of CO concentration at this amount during the period when the contaminant wave first reached the sensor. For experiments

C through H and J through M, the ambient CO concentration was less than 2 ppm. For experiments A, B, and I the ambient CO concentration was relatively high at 2 to 4 ppm of CO and was probably caused by heavier vehicular traffic near the mine portals during these experimental periods. Also shown in table 2 are the calculated travel times between sensors based upon entry volume only, τ_e, and based upon entry volume and dead-end crosscut volume, τ_{ec}. These travel times are calculated from the volumes under consideration divided by the volumetric flow rate, Q, in the following equations, $\tau_e = V_e/Q$, and $\tau_{ec} = V_{ec}/Q$, and assume no dispersion of CO occurs within the mine air. In other words, the calculated travel times assume the CO concentration within a volume of entry air does not vary with time as the air and CO move between entry sensors. These two travel times bracket the times produced by no entrainment of CO into the crosscuts and complete entrainment of CO into the crosscuts without CO dispersion along the entry.

The data in table 2 indicate that the presence of dead-end crosscuts between sensors generally results in a measured travel time of CO concentration between the sensors that is bounded by times calculated without and with crosscut volumes. These observations apply whether travel times based upon first arrival of CO or values of Δ5-ppm CO concentrations are considered. In experiment E, where all the crosscuts were isolated from the entries with brattices, there is substantial agreement between the measured travel times based upon arrival of Δ5-ppm CO at the sensors and the calculated values based upon entry volume (26 s compared with 26 s for the 5-to-18 path and 47 s compared with 50 s for the 12-to-4 path). Two of the measured travel times were slightly less than the calculated values for experiment E because of significant CO dispersion along the entry and because the first-arrival and the Δ5-ppm CO concentrations were less than half the maximum CO concentration. When the CO alarm concentration is less than half the maximum CO concentration in the entry, significant dispersion along the entry yields less of a travel time between two sensors than would have occurred if a square CO-concentration wave without significant dispersion moved between these two sensors.

Table 2.—Air velocity with measured and predicted CO travel times

Experiment	Path	Air velocity, m/s	Measured, s		Predicted, s	
			First arrival	Δ5-ppm	τ_e	τ_{ec}
A	5 → 18	1.14	42	45	31	44
	12 → 4	0.49	86	100	76	119
B	5 → 18	1.44	35	49	29	41
	12 → 4	0.77	71	84	54	85
C	5 → 18	1.53	28	34	25	36
	12 → 4	0.85	58	68	44	69
D	5 → 18	1.52	34	44	27	38
	12 → 4	0.76	54	57	49	77
E	5 → 18	1.78	24	26	26	26
	12 → 4	0.82	50	47	50	50
F	12 → 4	0.65	40	50	54	80
G	12 → 4	1.14	29	40	29	43
H	12 → 4	1.24	29	33	27	41
I	12 → 4	1.20	28	29	28	42
J	(8,9) → (16,17)	1.05	51	62	46	62
	(16,17) → (3,20)	1.10	31	30	27	35
	4 → (8,9)	1.08	9	15	9	34
K	(8,9) → (16,17)	1.01	48	52	48	64
	(16,17) → (3,20)	1.07	34	35	28	36
	4 → (8,9)	1.03	11	23	10	36
L	(8,9) → (16,17)	1.01	48	55	49	66
	(16,17) → (3,20)	1.04	32	46	29	37
	4 → (8,9)	1.04	17	28	10	35
M	(8,9) → (16,17)	0.84	57	45	60	60
	(16,17) → (3,20)	0.75	31	55	37	37
	4 → (8,9)	0.93	16	19	11	11

Notes: τ_e is the calculated CO travel time based on volume of entry.
τ_{ec} is the calculated CO travel time based on volume of entry and crosscuts.

Figure 10 shows a graph of τ_m versus τ_e and figure 11 shows a graph of τ_m versus τ_{ec} between sensors 5 and 18 and between sensors 12 and 4 for experiments A through I. It was found in the course of a sensor calibration that the calibration of the sensors was affected by the rotational orientation of the calibration plug in the sensor diffusion port for experiments A through G. The effect of this error in calibration on the concentration plots was to expand the concentration profiles for these experiments from curves to bands encompassing the original curves. These bands were not symmetrical about the original curves. Also, because of this calibration error, it was necessary to attach error bars to the data points in figures 10 and 11. The error bars represent the maximum possible excursions of the data from the most probable values, based upon postexperimental injection into the sensors of CO calibration gas for different rotational orientations of the calibration plug. The lines of perfect data correlation are the solid lines in figures 10 and 11. For these figures, three linear regressions of the data were made, one for the experimental data and one each for the upper and lower limits of the error bars.

Figure 10

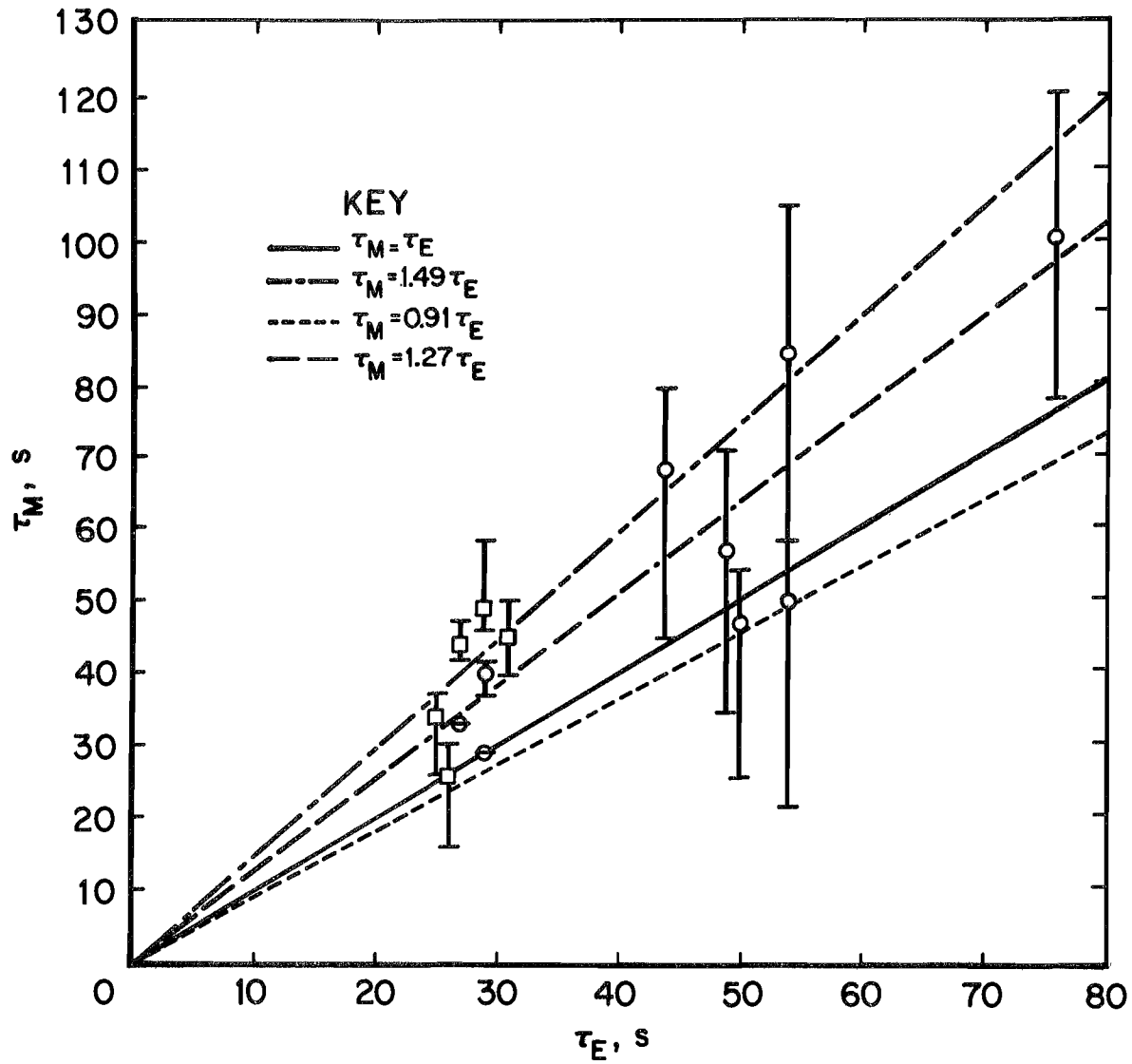

Measured travel time of 5-ppm CO between pairs of sensors versus calculated travel time not using crosscuts (□, sensor 5 to sensor 18; and ○, sensor 12 to sensor 4).

The regression lines in figure 10 form a wedge that is almost entirely above the line for perfect correlation. This implies the measured travel time between sensors is underestimated by the calculated travel time between sensors based only upon entry volume. The regression slope of the measured versus calculated travel time is 1.27. The regression lines in figure 11 form a wedge that is almost entirely below the line for perfect correlation. This implies the measured travel time between sensors is overestimated by the calculated travel time between sensors based upon entry and crosscut volume. For this case, the regression slope of the measured versus calculated travel time is 0.87. These figures show that the measured travel times for a 5-ppm-CO level are 27% greater than the calculated times based upon entry volume only, but 13% less than the calculated times based upon entry and crosscut volume. Future verification of these percentages in B and C Butts with a new and more accurate calibration apparatus is planned.

Figure 12 shows the results of experiments in F Butt performed after the calibration problem was solved. This figure compares the measured travel time with the calculated travel times, τ_e and τ_{ec}, for experiments J through M. The horizontal lines connect these two travel times for

Figure 11

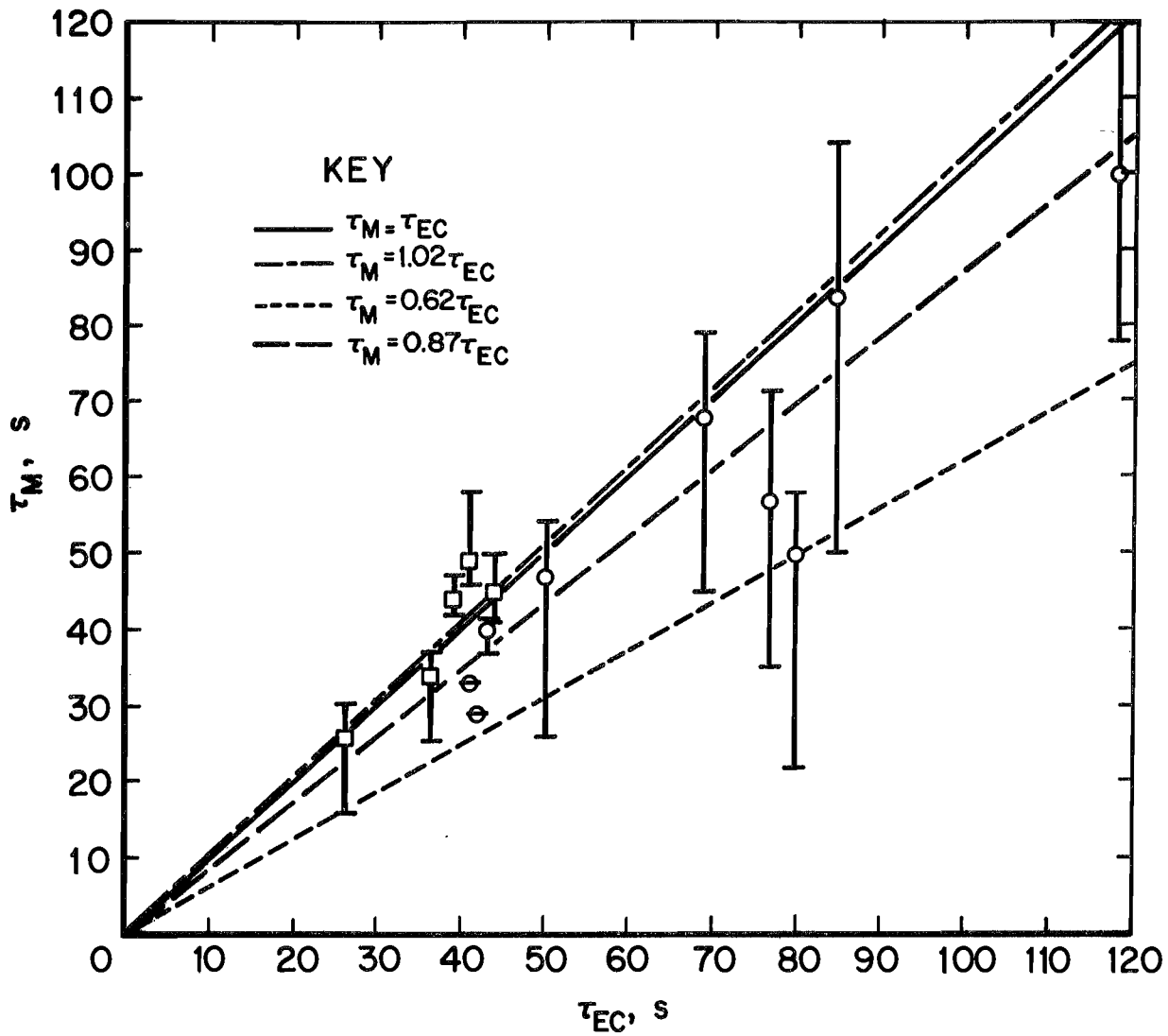

Measured travel time of 5-ppm CO between pairs of sensors versus calculated travel time using crosscuts (□, sensor 5 to sensor 18; and ○, sensor 12 to sensor 4).

Figure 12

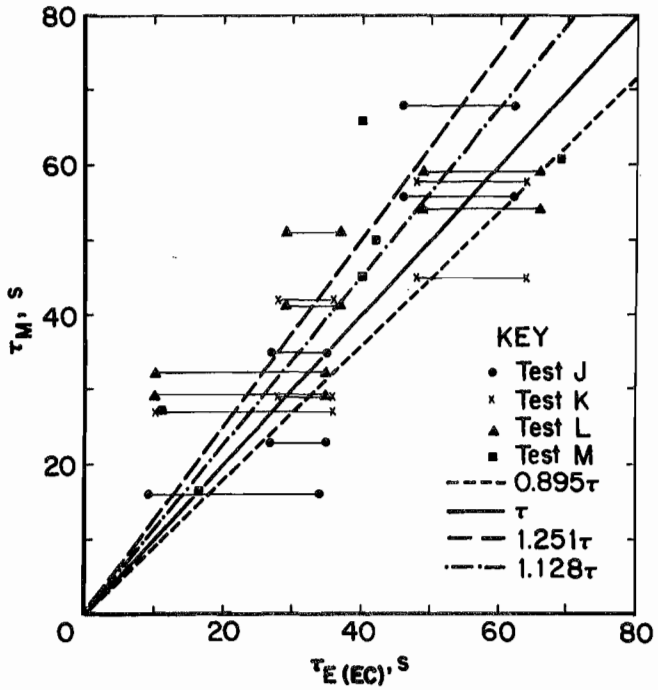

Measured travel times of 5-ppm CO versus calculated travel times after correcting calibration procedure.

experiments J to L. The two times are equivalent for experiment M in which all the crosscuts were bratticed off. These results estimate that the measured travel time for a 5-ppm-CO level is 25% greater than the calculated time based upon only entry volume, but 10% less than the calculated time based upon entry and crosscut volume. The results for these experiments with double-sided crosscuts are similar to the results with single-sided crosscuts.

The two experiments, E and M, with all the crosscuts bratticed off from the entry produced dissimilar results. A comparison between the measured and calculated travel times at the Δ5-ppm level in experiment E indicated, from a regression of the two measured times on the calculated times, a slope of 0.95, or that a typical measured time was 5% less than the calculated time. Possibly the dispersion effect predominated along B and C Butts. The results of experiment M indicated that, from a regression of six travel times measured along the entry, the measured time was 13% greater than the calculated time. The measured time would be greater than the calculated time if the effect of CO being diluted by air leaking into F Butt was greater than the dispersion effect.

Evaluation of higher levels of measured CO concentration, from 5 ppm above ambient up to the plateau concentration, showed that the measured travel time between sensors exceeded the calculated travel time based upon the total volume of entry and dead-end crosscuts. At higher concentrations of CO near the plateau region, the concentration curve can be highly nonlinear. Near the plateau region, with one sensor curve highly nonlinear, the upwind sensor curve can be essentially linear. Because of this possibility, it is recommended that interpretations of travel time between sensors be limited to the parts of the sensor curves where both curves exhibit essentially linear changes, which are usually near the curves' inflection points.

EMPIRICAL AND DISPERSION MODELS

The main variables perceived to influence the travel time between sensors, τ, were the volumetric flow rate, Q; the distance between sensors, L; the average cross-sectional area of the entry and crosscuts, A; the average height of the entry and crosscuts, H; the average width of the entry and crosscuts, W; the depth, B, of the crosscuts; and the number, n, of single-sided crosscuts. For double-sided crosscuts each side should be counted separately in determining the value of n. A dimensional analysis was performed to determine the best dimensionless combinations of these variables to correlate. The dimensionless term, $Q\tau/LA$, was assumed to be a function of the four, independent dimensionless variables, $(L+nB)/L$, B/W, H/W, and the Reynolds number in the entry. From 26 travel times measured in both single- and double-crosscut experiments that had little noise on the concentration curves, it was found that the only variable that was significantly functionally related to the term $Q\tau_m/LA$ was $(L+nB)/L$. For $Q\tau_m/LA$ versus $(L+nB)/L$ plotted on log-log coordinates in figure 13 (two points in figure 13 coincide), the following regression equations were determined:

$$\frac{Q\tau}{LA} = \left(\frac{L+nB}{L}\right)^{0.62}, \qquad (1)$$

or in terms of τ,

$$\tau = \left(\frac{LA}{Q}\right)\left(\frac{L+nB}{L}\right)^{0.62}. \qquad (2)$$

The 95% confidence interval for the exponent, 0.62, ranges from 0.52 to 0.71, assuming errors are normally

Figure 13

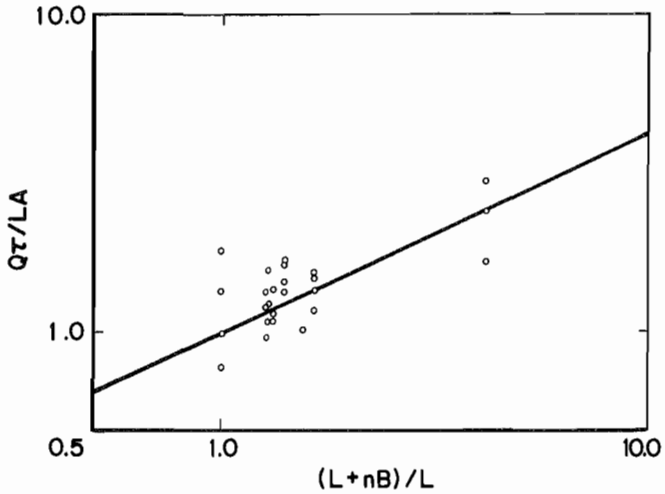

Correlation of $Q\tau/LA$ with $(L+nB)/L$, $Q\tau/LA = [(L+nB)/L]^{0.62}$.

distributed. The correlation coefficient for this regression is 0.76. The term, $A((L+nB)/L)^{0.62}$, from equation 2 corresponds to the effective, entry cross-sectional area suggested as an equation by Litton and others [(equation D-5) (*7*)]. The exponent, 0.5, in the equation of Litton and others (*7*) can be compared to the above exponent, 0.62, determined from measurements.

An analysis was made of the first two experiments described by Cohen (*3*) for travel times along a beltway in an operating mine with 10.4-m-deep double crosscuts. Sensors 3, 5, and 6 were located sequentially along the beltway. The distance between sensors 3 and 5 was 396 m. The distance between sensors 5 and 6 was 381 m. The average width and height of the beltway were 5.2 m and 2.1 m, respectively. The distance between the middle lines of the crosscuts was 25.9 m. The beltway ventilation had an average volumetric flow rate of 1,019 m^3/min. The measured travel times between sensors 3 and 5 were 6.5 min for experiment 1 and 5.6 min for experiment 2. The measured travel time between sensors 5 and 6 was 6.1 min for experiment 1. The travel times between 2-ppm-CO levels in experiment 1 and between 1.5-ppm-CO levels in experiment 2 were used for the measured values of τ. These low values of concentration were approximately equal to the ambient concentration plus half of the difference between the peak values and the ambient values. From this information, a least squares regression of the measured data results in an exponent of the right term in equation 1 of 0.63, nearly the same as the calculation based on the measurements in the SRCM.

In order to predict CO travel times based upon physical principles, a model of the dispersion of CO along an entry is needed. One model of the turbulent dispersion of CO along an entry requires knowing a coefficient of dispersion of CO. The determination of this coefficient for mine entries was partially addressed in previous research (*8*). For the experiments in this study, a method was devised to estimate the magnitude of this coefficient from the CO-sensor data. This method separated the intrinsic dynamics of the sensors from dynamics of the dispersion process along an entry with closed crosscuts. These dynamics of the dispersion process were then fit by an equation containing the dispersion coefficient. As described in appendix A, a dispersion coefficient of 1.5 m^2/s was determined from this method for the conditions within experiment M.

CONCLUSIONS

The results in figures 11 to 13 support the conjecture that the time for arrival of a specified CO concentration at a CO sensor is influenced by the dead-end crosscuts that adjoin the entry. It is possible to state generally that for the conditions of the above experiments, the travel time between sensors along an entry is bounded from below by a calculation that excludes crosscut volumes and from above by a calculation that includes crosscut volumes. This statement is accurate if the time rate of rise of the CO concentration above its ambient concentration is essentially constant. Furthermore, the travel time can be estimated quantitatively by the equation $\tau = LA((L+nB)/L)^{0.62}/Q$.

It was possible to approximate the measured change in concentration of a contaminant at a diffusion-type sensor by a sequential model that includes the sensor and the entry concentration dynamics. When CO was released into an entry, two first-order transfer functions in series, which constitute the sequential model, were fit to the mine-sensor data. Comparison between a mass-transfer dispersion model with the first-order model of the entry CO-concentration changes yielded, for this particular sensor, a best fit dispersion coefficient of 1.5 m^2/s.

This investigation has provided a correlation for use in the estimation of a mine fire's location as part of a fire-location model and a methodology for a parameter

estimation. The results for mines with single and double crosscuts also could be used in a fire-location model to bracket the contaminant travel times by 27% (crosscuts excluded) and -13% (crosscuts included), and in turn to bracket the distances that would contain the location of the fire. Another realization of this investigation is that the time to a fire alarm from a mine-monitoring system can be reduced if it is practical to brattice off unused crosscuts at the entry rather than deep within the crosscuts.

REFERENCES

1. Laage, L. W., W. H. Pomroy, and A. Bartholomew. Computer-Aided Underground Mine Fire Location. Paper in Proceedings of the 23rd International Conference of Safety in Mines Research Institutes (Washington, DC, Sept. 11-15, 1989). USBM, pp. 1028-1037.

2. Edwards, J. C. Fire Location Model. USBM IC 9261, 1990, 14 pp.

3. Cohen, A. F. Ventilation Code Predictions Versus Measured First Contaminant Arrival Times for Coal Mine Fires in Belt Entries. Paper in Proceedings of the International Symposium on Mine Mechanization and Automation, vol. II, June 10-13, 1991. CO School of Mines, 1991, pp. 13-62.

4. Edwards, J. C., and R. E. Greuer. Real-Time Calculation of Product-of-Combustion Spread in a Multilevel Mine. USBM IC 8901, 1982, 117 pp.

5. Edwards, J. C., and Jing-Shu Li. Computer Simulation of Ventilation in Multilevel Mines. Paper in Mine Ventilation ed. by M. J. Howes and M. J. Jones (Proc. 3rd International Mine Ventilation Congress, London, England, June 13-19, 1984). Inst. Min. and Metall., 1984, pp. 47-51.

6. Ouderkirk, S. J., W. H. Pomroy, J. C. Edwards, and J. Marks. Mine Stench Fire Warning Computer Model Development and In-Mine Validation Testing. Paper in Mine Ventilation ed. by P. M. Jones (Proc. 2nd U.S. Mine Ventilation Symp., Reno, NV, Sept. 23-25, 1985). A. A. Balkema, 1985, pp. 29-35.

7. Litton, C. D., C. P. Lazzara, and F. J. Perzak. Fire Detection for Conveyor Belt Entries. USBM RI 9380, 1991, 23 pp.

8. Stefanov, T. P., E. D. Vlasseva, and E. E. Arenyan. Unsteady Gas Flows in Mine Ventilation Networks. Paper in Proceedings of the 22nd International Conference of Safety in Mines Research Institutes (Beijing, China). China Coal Industry Publishing House, Oct. 1987, pp. 115-122.

9. Jost, W. Diffusion In Solids, Liquids, and Gases. Academic Press, 1960, p. 47.

10. Carslaw, H. S., and J. C. Jaeger. Conduction of Heat in Solids. Clarendon Press, 1959, p. 388.

APPENDIX A.—DISPERSION MODEL

In order to separate the dispersion effect from the entrainment effect along an entry with crosscuts, an analysis was made of the measured CO concentration from an entry sensor within experiment M that had all crosscuts brattice off from the entry. The data from sensor 16 were chosen because of the relative lack of noise in its plot and the large distance between this sensor and the injector. These data are shown, shifted downward so the ambient concentration is 0 ppm, as the measured curve in figure A-1. By letting t_0 be the first-arrival time of CO at a sensor, this particular sensor began to respond to CO concentration above the ambient level at t_0 = 82 s. The sensor had intrinsic dynamics that were well approximated by a first-order, ordinary differential equation with a characteristic time constant, α_1, shown by the following equation:

$$\alpha_1 \left[\frac{dC_s}{dt}\right] + C_s = C_f, \qquad \text{(A-1)}$$

where $C_s(t)$ is the sensor response to an increase in CO concentration, C_f, from $C_s(t_0) = 0$. The time constant was determined from an exposure of the sensor to a step increase in CO concentration in the calibration mode. This time constant, α_1 = 30 s, was the difference between the time of injection of the calibration gas and the time required for the sensor to indicate about 63.2% of its final value. The sensor response, $C_s(t)$, to the step change in CO concentration is shown in figure A-1.

The CO dispersion along the entry was also approximated by a first-order, ordinary differential equation with an unknown time constant, α_2, which was dependent upon the shape of the curve from sensor-16 data. A combination of these two first-order, sequential processes yields a model for the measured mine concentration. As an approximation to the measured mine concentration, $C_m(t)$, is the solution to the following second-order, ordinary differential equation:

$$\alpha_1\alpha_2 \frac{d^2C_m}{dt^2} + (\alpha_1+\alpha_2) \frac{dC_m}{dt} + C_m = C_f, \qquad \text{(A-2)}$$

where $C_m(t)$ has the initial conditions of $C_m(t_0) = 0$ and $dC_m(t_0)/dt = C^1_i$. The solution to the above differential equation is the following equation for $t \geq t_0$,

$$C_m = C_f \left[1 - \left[\frac{1}{\alpha_2-\alpha_1}\right] \left[\left[\frac{\alpha_2(C_f - \alpha_1 C^1{}_i)}{C_f}\right] e^{(t_0-t)/\alpha_2} - \left[\frac{\alpha_1(C_f - \alpha_2 C^1{}_i)}{C_f}\right] e^{(t_0-t)/\alpha_1}\right]\right]. \qquad \text{(A-3)}$$

Figure A-1

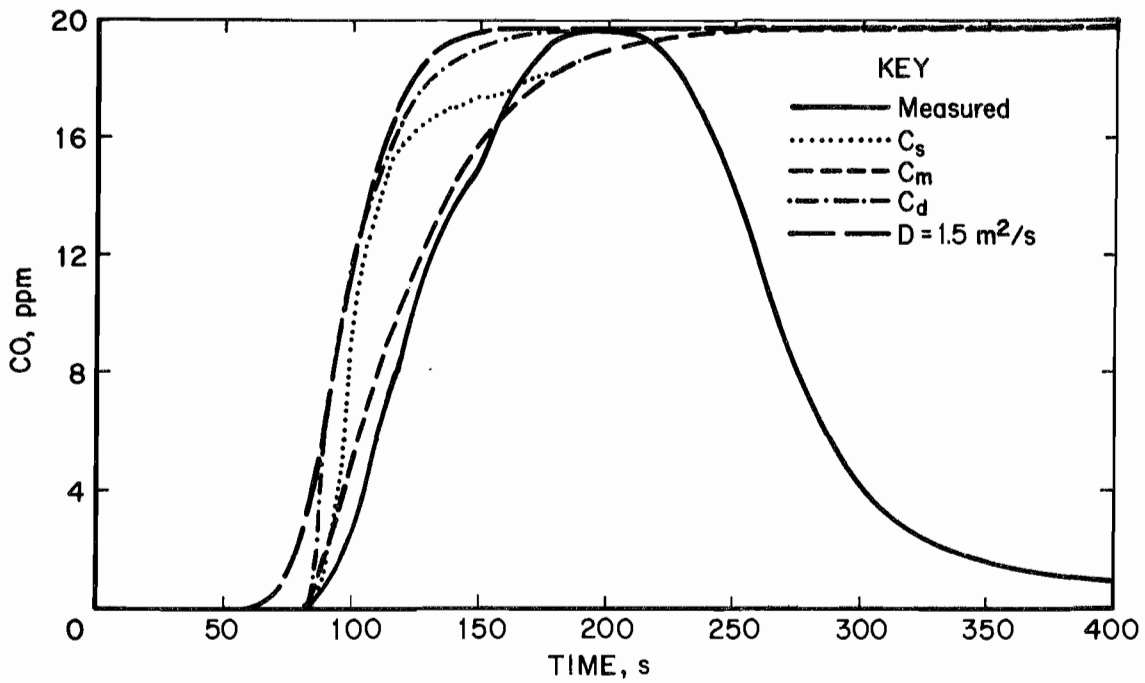

Estimate of dispersion coefficient from CO concentration at sensor 16 in F Butt for experiment M.

For the application of the above equation to the concentration curve at sensor 16 in experiment M, the following values were measured: C_f = 19.7 ppm, and C^1_i = 0.22 ppm/s. The best subjective fit of the above equation for t ≥82 s to the mine concentration curve was obtained by setting α_2 = 20 s and is shown in figure A-1. Once this optimal value of α_2 was determined, a first estimate to the dispersion process is given by the following equation for t ≥82 s,

$$C_d = C_f \left(1 - e^{(t_0-t)/\alpha_2}\right), \qquad \text{(A-4)}$$

where $C_d(t)$ is the concentration of CO without the effect of sensor dynamics. Equation A-4 would be the same as equation A-3 if the time constant, α_1, was 0 in equation A-2. Equation A-4 constitutes a first model for contaminant dispersion. The curve for $C_d(t)$ is shown in figure A-1.

A second, more accurate model of CO transport and dispersion was developed that uses the results of the first model. This second model is based upon forced-convective transport and dispersion of CO at an average air velocity, u, and a turbulent dispersion of CO characterized by a constant dispersion coefficient, D. This one-dimensional, mass-transfer model for the transport of CO along an entry without crosscuts is given by the following partial differential equation (*9*):

$$\frac{\partial C}{\partial t} = D\frac{\partial^2 C}{\partial x^2} - u\,\frac{\partial C}{\partial x}, \qquad \text{(A-5)}$$

where x is the distance from the injector, C(x,t) = 0 for $t < t_1$, C(0,t) = C_f for $t \geq t_1$, and C(∞, t) = 0. The above equation is derived from a mass balance for CO along the entry. The first term is proportional to the accumulation of mass at any distance along the entry, the second term is proportional to the net flow rate of mass from CO dispersion, and the last term is proportional to the net bulk flow rate of CO along the entry. The time, t_1, was chosen so the curves from the two CO-transport models would approximately coincide at a CO concentration of $C_f/2$. It is calculated from the difference between the time, $t_0 + \alpha_2 \ln 2$, for the concentration predicted by the first model to reach $C_f/2$, 9.85 ppm, and the bulk-flow transport time, I_1/u_1, where I_1 is the distance between the injector and sensor 16, 67.4 m, and u_1 is the average air velocity in F Butt during experiment M, 0.9 m/s. Formally, this is expressed by this equation:

$$t_1 = t_0 + \alpha_2 \ln 2 - I_1/u_1 . \qquad \text{(A-6)}$$

From the parameter values in the first model, $t_0 + \alpha_2 \ln 2$ = 95.9 s for the concentration, $C_d(t)$, to reach 9.85 ppm. Application of equation A-6 to the values above yields t_1 = 21 s. The solution (*10*) to the one-dimensional model, equation A-5, is given by the following equation:

$$C = \left[\frac{C_f}{2}\right]\left[\operatorname{erfc}\left[\frac{x-u(t-t_1)}{2\sqrt{D(t-t_1)}}\right] + e^{(ux/D)}\operatorname{erfc}\left[\frac{x+u(t-t_1)}{2\sqrt{D(t-t_1)}}\right]\right], \qquad \text{(A-7)}$$

where erfc is the complimentary error function. The dispersion coefficient, D, was determined to be 1.5 m^2/s with $u = u_1$ from a trial-and-error search for a best fit of $C(I_1,t)$ from the second model to $C_d(t)$ from the first model. The result of this curve fitting is shown in figure A-1. The slopes of $C(I_1,t)$ and $C_d(t)$ are very similar in the region near the concentration of $C_f/2$ = 9.85 ppm. Figure A-2 shows the sensitivity of the second model to slight variations in D from 0.9 m^2/s to 2.2 m^2/s.

Figure A-2

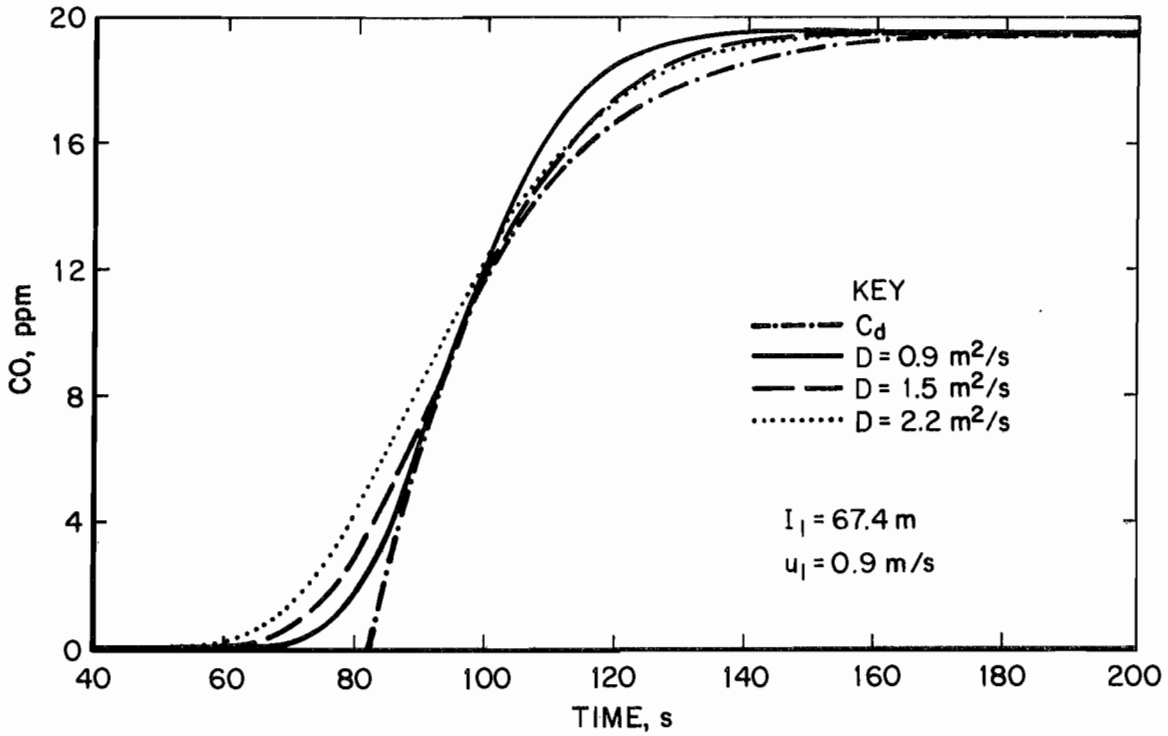

Effect of variation of CO dispersion coefficient on shape of modeled CO-concentration curve.

APPENDIX B.—LIST OF SYMBOLS

A	average cross-sectional area of entry and crosscuts, m^2
A_c	cross-sectional area of crosscut, m^2
A_e	cross-sectional area of entry, m^2
B	depth of crosscut, m
C	contaminant concentration from second model, ppm
C_d	contaminant concentration from first model, ppm
C_m	contaminant concentration from mine model, ppm
C_s	contaminant concentration from sensor response, ppm
C^1_i	time rate of change of contaminant concentration, ppm/s
D	dispersion coefficient, m^2/s
E	enthalpy, calories/g
H	average height of entry and crosscuts, m
I	distance between injector and sensor, m
L	distance between sensors, m
n	number of one-sided crosscuts
P	gas pressure, kPa
Q	volumetric flow rate of air, m^3/s
T	gas temperature, degree Kelvin
t	time from start of contaminant injection, s
t_0	first-arrival time of contaminant at sensor, s
t_1	modeled, injected-contaminant start time, s
u	average velocity of air in entry, m/s
V_c	volume of crosscuts between sensors, m^3
V_e	volume of entry between sensors, m^3
V_{ec}	volume of entry and crosscuts between sensors, m^3
W	average width of entry and crosscuts, m
x	distance from injector, m
α_1	time constant of sensor, s
α_2	time constant of first model, s
Δ	concentration change above ambient concentration, ppm
τ	calculated contaminant travel time from correlation, s
τ_e	calculated contaminant travel time based on volume of entry, s
τ_{ec}	calculated travel time based on volume of entry and crosscuts, s
τ_m	experimentally measured contaminant travel time, s